Biomass burning pollution in the South Atlantic upper troposphere: GLORIA trace gas observations and evaluation of the CAMS model

Sören Johansson[1], Gerald Wetzel[1], Felix Friedl-Vallon[1], Norbert Glatthor[1], Michael Höpfner[1], Anne Kleinert[1], Tom Neubert[2], Björn-Martin Sinnhuber[1], and Jörn Ungermann[3]

[1]Institute of Meteorology and Climate Research - Atmospheric Trace Gases and Remote Sensing (IMK-ASF), Karlsruhe Institute of Technology, Karlsruhe, Germany
[2]Central Institute of Engineering, Electronics and Analytics - Electronic Systems (ZEA-2), Forschungszentrum Jülich, Jülich, Germany
[3]Institute of Energy and Climate Research - Stratosphere (IEK-7), Forschungszentrum Jülich, Jülich, Germany

Correspondence: S. Johansson (soeren.johansson@kit.edu)

Abstract. In this study, we present simultaneous airborne measurements of peroxyacetyl nitrate (PAN), ethane (C_2H_6), formic acid (HCOOH), methanol (CH_3OH), and ethylene (C_2H_4) above the South Atlantic in September and October 2019. Observations were obtained from the Gimballed Limb Observer for Radiance Imaging of the Atmosphere (GLORIA), as two-dimensional altitude cross-sections along the flight path. The flights were part of the SouthTRAC (Transport and Composition
5   in the Southern Hemisphere Upper Troposphere/Lower Stratosphere) campaign with the German High Altitude and Long range research Aircraft (HALO). On two flights (8 September 2019 and 7 October 2019), large enhancements of all these substances were found between 7 and 14 km altitude with maximum volume mixing ratios (VMRs) of 1000 pptv of PAN, 1400 pptv for C_2H_6, 800 pptv for HCOOH, 4500 pptv for CH_3OH, and 200 pptv for C_2H_4. One flight shows a common filamentary structure in the trace gas distributions, while the second flight is characterized by one large plume. Using backward trajectories,
10   we show that measured pollutants are likely originating from South America and central Africa, where elevated PAN VMRs are visible at the surface layer of the Copernicus Atmosphere Monitoring Service (CAMS) model during the weeks before both measurements. In comparison to simulation results of the CAMS reanalysis interpolated onto the GLORIA measurement geolocations, we show that the model is able to reproduce the overall structure of the measured pollution trace gas distributions. For PAN, the absolute VMRs are in agreement with the GLORIA measurements, too. However, C_2H_6 and HCOOH are
15   generally underestimated by the model, while CH_3OH and C_2H_4, the species with the shortest atmospheric lifetimes of the discussed pollution trace gases, are overestimated by CAMS. The good agreement between model and observations for PAN suggests that the general transport pathways and emissions locations are well captured by the model. The poorer agreement for other species is therefore most likely linked to model deficiencies in the representation of loss processes and emission strength.

1 Introduction

20   The composition of the upper troposphere and lower stratosphere (UTLS) above South America and even above remote regions of the South Atlantic is strongly influenced by frequent biomass burning events in central Africa, South America, and

Australia (e.g., Andreae and Merlet, 2001; Glatthor et al., 2015). Pollution trace gases and aerosols, resulting from fires, can be transported to the UTLS. Here, some of these trace gases are able to produce ozone (O_3), which acts as efficient greenhouse gas at these altitudes (Xia et al., 2017). Further, some pollution trace gases may act as aerosol precursor (e.g., Lim et al., 2019).

25 Together with directly emitted aerosols, they influence surface climate. It is well known that the UTLS is of great importance for global climate (Gettelman et al., 2011; Riese et al., 2012), and it is thus important to study biomass burning trace gases at UTLS altitudes. Due to increasing biomass burning activities in Africa, South America and Australia (Torres et al., 2010; Abram et al., 2021), their potential influence on climate is increasing, too.

Typical biomass burning trace gases have different atmospheric lifetimes, atmospheric sinks and may have other than py-

30 rogenic sources. In this work, peroxyacetyl nitrate (PAN), ethane (C_2H_6), formic acid (HCOOH), methanol (CH_3OH), and ethylene (C_2H_4) are discussed, and their characteristics are summarized in Tab. 1. These trace gases have been observed by several satellite instruments in nadir (e.g., Coheur et al., 2009; Dolan et al., 2016; Franco et al., 2018; Pope et al., 2021) as well as in limb views (e.g., Rinsland et al., 2005; Dufour et al., 2007; Grutter et al., 2010; Wiegele et al., 2012). These measurements allowed for monitoring of large scale biomass burning plume transport and chemical composition. In addition, airborne in situ

35 (e.g., Singh et al., 2001; Peischl et al., 2018) and remote sensing (e.g., Ungermann et al., 2013; Johansson et al., 2020; Wetzel et al., 2021) observations provided detailed studies of filamentary structures of these pollution trace gases.

Atmospheric simulations of such pollution trace gases are challenging: Biomass burning events are typically represented by emission data sets in atmospheric models. If major fire events are missing in these emissions, the model is not able to reproduce upper tropospheric distributions of those species. Further, injection heights of polluted air masses from fires are

40 difficult to estimate, and only few emission data sets include this information (e.g., Rémy et al., 2017). In addition, it is difficult to estimate the type of fuel of biomass burning events, and thus the knowledge of the concentration of the emitted compounds is uncertain (e.g., van der Werf et al., 2017). Another challenge is to simulate transport pathways of polluted air masses due to pyroconvective updraft (e.g., Khaykin et al., 2020). Furthermore, atmospheric processes, which are relevant for these biomass burning pollution trace gases, are subject of recent research, like the formation of HCOOH (Franco et al., 2021). For example,

45 Wetzel et al. (2021) showed that it is difficult to reproduce measured pollution trace gas plumes above the North Atlantic without artificially enhanced emissions. Earlier, Coheur et al. (2007) compared ACE-FTS observations of a biomass burning plume with their model and found considerable differences in the vertical profiles of carbon monoxide (CO).

Between September and November 2019, the SouthTRAC (Transport and Composition in the Southern Hemisphere Upper Troposphere/Lower Stratosphere) aircraft campaign was conducted with base in Rio Grande, Argentina. Onboard the German

50 research aircraft HALO (High Altitude and Long range research aircraft), ten in situ and three remote sensing instruments performed measurements during transfer flights from Oberpfaffenhofen, Germany to Rio Grande, Argentina, and during local flights from Rio Grande. The GLORIA (Gimballed Limb Observer for Radiance Imaging of the Atmosphere) instrument was part of the HALO payload and measured two dimensional distributions of temperature and various trace gases, such as PAN, C_2H_6, HCOOH, CH_3OH, and C_2H_4, along the flight track. In this work, we use these measurements to identify polluted air

55 masses, estimate their origins using backward trajectories and perform quantitative comparisons of the measurements with the CAMS (Copernicus Atmosphere Monitoring Service) model simulation results.

Table 1. Sources, sinks, estimated lifetimes, and approximate upper tropospheric background volume mixing ratios (VMRs) of pollution trace gases PAN, C_2H_6, HCOOH, CH_3OH, and C_2H_4 which are discussed in this paper.

	Sources	Sinks	Lifetime	Background VMRs	References
PAN	Precursors:	Thermal decomposition	1 h (BL)	<100 pptv	Fischer et al. (2014)
	Fuel combustion	Photolysis (UT)	5 months (UT)		Glatthor et al. (2007)
	Biomass burning				
C_2H_6	Biomass burning	Reaction with OH	2 months	<500 pptv (NH)	Rudolph (1995)
	Natural gas loss			<300 pptv (SH)	Xiao et al. (2008)
	Fossil fuel production				
	Bio fuel use				
HCOOH	Biogenic emissions	Reaction with OH	1-2 days (BL)	<100 pptv	Paulot et al. (2011)
	Biomass burning	Wet and dry deposition	weeks (UT)		Millet et al. (2015)
	Fossil fuel combustion				Mungall et al. (2018)
	Secondary production				
CH_3OH	Biogenic emissions	Reaction with OH	5.3 days	<300 pptv	Bates et al. (2021)
	Oceanic emissions	Wet and dry deposition			
	Biomass burning	Ocean uptake			
	Anthropogenic emissions				
	Secondary production				
C_2H_4	Biogenic emissions	Reaction with OH	0.5 days (LT)	<50 pptv	Sawada and Totsuka (1986)
	Biomass burning	Reaction with O_3	1.2 days (UT)		Mauzerall et al. (1998)
	Fossil fuel combustion				Morgott (2015)

BL - boundary layer; LT - lower troposphere; UT - upper troposphere; NH - northern hemisphere; SH - southern hemisphere

In the following, we present an overview of GLORIA measurements and retrievals during the SouthTRAC campaign, together with a description of the atmospheric models used by this study. Then, the measured concentrations of biomass burning trace gases for two research flights above the South Atlantic are discussed in detail, followed by a backward trajectory analy-
60 sis to estimate the origin of biomass burning plumes. Finally, GLORIA observations are directly compared to CAMS model simulation results.

2   Observations and atmospheric model simulations

2.1   GLORIA measurements during the SouthTRAC aircraft campaign

The GLORIA instrument (Friedl-Vallon et al., 2014; Riese et al., 2014) has been deployed on various aircraft campaigns with
65 the Russian M55 Geophysica (e.g., Höpfner et al., 2019) and the German HALO research aircraft (e.g., Oelhaf et al., 2019). The instrument combines a Fourier-Transform-Spectrometer with an imaging detector, which allows for simultaneous obser-

Table 2. Retrieval properties for PAN, C_2H_6, HCOOH, CH_3OH, and C_2H_4: Spectral regions used, and handling of interfering species. 10 and 90 percentile ranges are given for vertical resolution and estimated errors. In the supplement, it is shown that larger absolute errors are typically connected to higher VMRs.

Target gas	Spectral regions	Fitted species	Forward-calculated species	Vert. resolution	Estimated error
PAN	780.0 - 790.0 cm^{-1} 794.0 - 805.0 cm^{-1}	$H_2O^{\dagger}$, $O_3^{\dagger}$, HCFC-22, CCl_4, PAN	CO_2, NO_2, NH_3, $HNO_3^{\dagger}$, ClO, OCS, HCN, CH_3Cl, C_2H_2, C_2H_6, COF_2, C_2H_4, CFC-11†, CFC-113, CFC-141, $ClONO_2^{\dagger}$, CH_3OH, HNO_4, CH_3COCH_3	0.4 - 0.8 km	40 - 130 pptv
C_2H_6	819.000 - 822.625 cm^{-1} 829.750 - 833.125 cm^{-1}	$O_3^{\dagger}$, C_2H_6, HCFC-22	$H_2O^{\dagger}$, CO_2, NO_2, NH_3, $HNO_3^{\dagger}$, HCN, CH_3Cl, C_2H_2, COF_2, CFC-11†, CCl_4, $ClONO_2^{\dagger}$, CH_3CCl_3, PAN	0.8 - 1.1 km	130 - 380 pptv
HCOOH	1086.50 - 1089.44 cm^{-1} 1103.50 - 1106.12 cm^{-1} 1112.50 - 1116.88 cm^{-1}	HCOOH, $O_3^{\dagger}$, CFC-12†, HCFC-22	$H_2O^{\dagger}$, CO_2, NH_3, CFC-11†, CFC-113, CFC-114	0.5 - 1.2 km	30 - 140 pptv
CH_3OH	982.875 - 999.312 cm^{-1}	$H_2O^{\dagger}$, $O_3^{\dagger}$, NH_3, CH_3OH, PAN	CO_2, CFC-113	0.4 - 0.9 km	200 - 680 pptv
C_2H_4	945.188 - 952.312 cm^{-1}	$H_2O^{\dagger}$, NH_3, C_2H_4, SF_6	CO_2, $O_3^{\dagger}$, N_2O, NO_2, $HNO_3^{\dagger}$, COF_2, CFC-11†, CFC-12†, HCFC-22, CH_3CCl_3, CH_3COCH_3, PAN	0.3 - 0.7 km	30 - 110 pptv

† Results of previous retrievals (not shown in this paper) targeting these species have been used for simulation of the spectra, or as an initial guess for the retrieval.

vations of 128×48 atmospheric spectra. An actively controlled gimbal frame enables compensation of aircraft movements and targeted line of sight control. Two external black bodies as well as measurements into deep space are used for in-flight radiometric calibration. In this study, we use interferograms recorded in GLORIA's high-spectral-resolution mode. This mode

70 utilizes an optical path difference of 8.0 cm, which results in spectral sampling of 0.0625 cm^{-1}, and a horizontal sampling along the flight path of approximately 3.5 km. These recorded interferograms are radiometrically and spectrally calibrated according to GLORIA level 1 processing as described by Kleinert et al. (2014), Guggenmoser et al. (2015), and Ungermann et al. (2021). The spectra are horizontally binned after filtering of bad pixels, such that the final data product is a set of 127 vertical spectra per measurement (one row is filtered completely).

75 These calibrated spectra are then used to retrieve atmospheric profiles of temperature, aerosols and trace gases. The retrieval applies a nonlinear least-squares fit algorithm with Tikhonov regularization, and is based on the retrieval strategy as described by Johansson et al. (2018). Overall, the retrievals are similar to retrievals of pollution trace gases as described by Wetzel et al. (2021) and Johansson et al. (2020). Specific retrieval properties are summarized in Tab. 2. Detailed error estimation and vertical resolution analyses are provided as supplement to this paper, and a summary per species is presented in Tab. 2. Spectroscopic

80 errors are noted in the supplement and are, among other sources, based on uncertainties reported by Rothman et al. (2005) and Gordon et al. (2017).

GLORIA observations used in this study were recorded during the SouthTRAC HALO aircraft campaign. This campaign was conducted in two phases between September and November 2019, of which the phase in September focused on measurements of gravity waves (Rapp et al., 2021). GLORIA measurements have been obtained during transfer flights between

85   Oberpfaffenhofen, Germany, and Rio Grande, Argentina, and local flights from Rio Grande. In this study, results from two transfer research flights are discussed. The flights on 8 September 2019 and 7 October 2019 were directed from Sal, Cape Verde to Buenos Aires, Argentina, and vice versa, as part of the aircraft transfer between Germany and Rio Grande. Those flights have been selected for this study, because they covered the UTLS region above the South Atlantic and revealed the highest volume mixing ratios of the examined pollution trace gases.

90   ## 2.2 CAMS atmospheric model

The Copernicus Atmosphere Monitoring Service (CAMS) provides the ECMWF (European Centre for Medium-Range Weather Forecast) Atmospheric Composition Reanalysis version 4 (EAC4) data product (Flemming et al., 2015; Inness et al., 2019). This data product (in this manuscript abbreviated as "CAMS") utilizes the ECMWF Integrated Forecast System (IFS) model, which assimilates various observations of atmospheric state and composition. The model applies a chemistry module named

95   IFS(CB05) (Flemming et al., 2015) and an aerosol module as described by Morcrette et al. (2009). The model has 60 vertical levels between 0.1 hPa and 1000 hPa, and has a horizontal resolution of $0.75° \times 0.75°$ latitude $\times$ longitude. Output is provided every 3 h and includes a variety of meteorological parameters, concentrations of chemical tracers, and aerosol properties for the time between 2003 and 2020. CAMS uses prescribed emissions from MACCity (MACC/CityZEN; Granier et al., 2011) for anthropogenic emissions, from MEGAN2.1 (Model of Emissions of Gases and Aerosols from Nature; Guenther et al.,

100   2012) for biogenic emissions, and from GFAS v1.2 (Global Fire Assimilation System; Kaiser et al., 2012) for biomass burning emissions. GFAS assimilates information of fire radiative power and injection height from satellite observations. In a model evaluation study, Wang et al. (2020) compared tropospheric trace gas profile measurements from aircraft campaigns to CAMS reanalysis data. They compared measurements taken over the Arctic, North America and Hawaii to model simulation results and show that simulated PAN is in agreement with observations, while CAMS C_2H_6 is generally underestimated. Because

105   this evaluation is limited to the northern hemisphere and does not capture large scale biomass burning events, our manuscript may contribute to estimate the general performance of CAMS in reproducing pollution trace gas distributions in the upper troposphere.

2.3 HYSPLIT trajectory model

The HYbrid Single-Particle Lagrangian Integrated Trajectory model (HYSPLIT; Stein et al., 2015; Rolph et al., 2017) is a

110   commonly used transport and dispersion model developed by the Air Resources Laboratory of the National Oceanic and Atmospheric Administration. In this work, we use HYSPLIT to calculate backward trajectories based on Global Forecast System (GFS) global model results with a horizontal resolution of $0.25° \times 0.25°$ latitude $\times$ longitude. Seven day backward trajectories are started at measurement geolocations with enhanced pollution trace gas signatures in the GLORIA measurements. Upward transport of the trajectories is limited to the vertical motion prescribed by the meteorological fields. It is well known that these

115 meteorological fields underestimate upward transport, in particular for convective events, which are usually not resolved or sufficiently parameterized by meteorological models (e.g., Hoyle et al., 2011). Advanced schemes for convection detection along backward trajectories (e.g., Wohltmann et al., 2019) are not applied for backward trajectories used by this study. For this reason, the vertical motion of the HYSPLIT trajectories is not analyzed in detail here.

3 Pollution trace gas measurements

3.1 Flight on 8 September 2019

120 The SouthTRAC research flight on 8 September 2019 was part of the transfer of the HALO aircraft from Oberpfaffenhofen, Germany to Rio Grande, Argentina and started in Sal, Cape Verde in southwest direction towards Buenos Aires, Argentina. Figure 1a shows the flight track as well as PAN VMRs at the horizontal tangent point locations of the GLORIA field of view. To facilitate the interpretation of the trace gas cross sections in the following panels, measurement times are also indicated. Fire

125 events in South America and Africa during three days before the GLORIA measurements, obtained from the Fire Information for Resource Management System (FIRMS) are shown as red dots in the background of the map. These data are based on observations from the Moderate Resolution Imaging Spectroradiometer (MODIS) onboard the NASA Terra and Aqua satellites and are shown here to provide an overview of biomass burning events prior to the research flight. These fire data reveal a large density of fires in central South America. Furthermore, horizontal winds at 250 hPa (approximately 10 km altitude) from the

130 fifth generation of the ECMWF Reanalysis (ERA5) are shown as colored arrows to provide meteorological context of the GLORIA measurements. These horizontal winds indicate strong south-westerly currents reaching the flight path at the equator (approximately 7:00 UTC). Another region of strong winds is located above the South Atlantic with north-westerlies parallel to the flight path. Above the South American continent, where many fire counts are displayed, weaker north-westerly winds are marked, which may transport polluted air from the fires to the measurement locations. However, these winds, which are

135 only shown at 250 hPa, can only provide a simple overview of the situation, which will be more closely analysed by trajectory calculations below.

The measured cross sections of the pollution trace gases reveal filamentary structures along the flight path. At the beginning of the flight around 7:00 UTC, two layers of enhanced pollution trace gas concentrations are observed at altitudes of 8 km and 11 km for all discussed trace gases, except C_2H_4 (marked by orange and cyan boxes). Compared to other enhancements

140 during this flight, these local maxima are relatively low (up to 500 pptv for PAN, 700 pptv for C_2H_6, 300 pptv for HCOOH, and 1200 pptv for CH_3OH, Fig. 1b-e). During the later part of the flight, strong enhancements of PAN of up to 900 pptv are measured at 8:00 UTC and 13 km altitude (green). These air masses also contain strongly enhanced C_2H_6 (up to 1000 pptv), weaker enhanced HCOOH (up to 500 pptv) and CH_3OH (up to 2000 pptv), but no signatures of enhanced C_2H_4. At the same time, but at lower altitudes of around 8 km (magenta), a weaker local maximum is observed for PAN (up to 500 pptv), C_2H_6

145 (up to 1100 pptv), HCOOH (up to 400 pptv), and CH_3OH (up to 1600 pptv), but again not for C_2H_4. Later during the flight, at 9:15 UTC and 10 km altitude (yellow), a strong enhancement is measured for all five discussed trace gases (up to 1000 pptv for PAN, 900 pptv for C_2H_6, 800 pptv for HCOOH, 4000 pptv for CH_3OH, and 200 pptv for C_2H_4). Above this horizontally
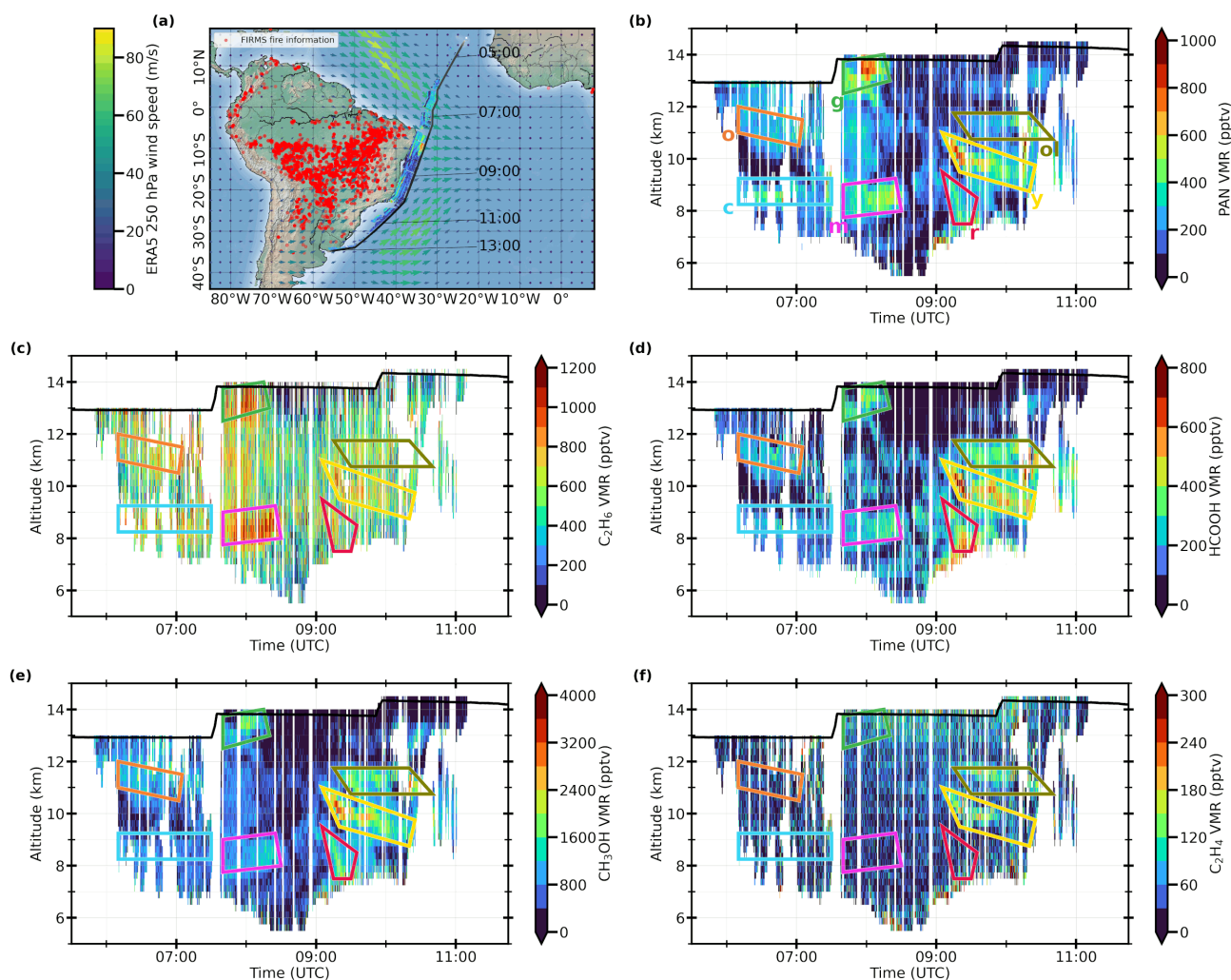
Figure 1. (a) Flight path for SouthTRAC research flight on 8 September 2019 from Sal, Cape Verde to Buenos Aires, Argentina. Along the flight track, concentrations of PAN are displayed at the horizontal distributions of the tangent points (colorbar in b). The temporal evolution of the flight is indicated by times in UTC, marked along the flight track. Fire events as noted by FIRMS during 3 days before the GLORIA measurements are indicated as red dots on the map. ERA5 horizontal winds at 8:00 UTC at a typical measurement altitude of 250 hPa (approximately 10 km) are shown as arrows with amplitudes given by the left colorbar. (b) Vertical distribution of GLORIA measurements of PAN for SouthTRAC flight on 8 September 2019. The black line marks the aircraft altitude. Colored boxes mark air masses of interest, which are discussed in more detail by a trajectory analysis in the following section (o: orange, c: cyan, g: green, m: magenta, ol: olive, y: yellow, r: red). (c) Same as (b), but for C_2H_6. (d) Same as (b), but for HCOOH. (e) Same as (b), but for CH_3OH. (f) Same as (b), but for C_2H_4.

extending local maximum, a similar structure is observed at 11 km altitude (olive). For all measured trace gases but C_2H_4, absolute VMRs are smaller compared to the enhancement at 10 km altitude. Again, at 9:15 UTC but at altitudes above cloud

150 tops (7 km; red), a local enhancement with smaller absolute VMRs is measured for all discussed trace gases, except C_2H_4. Towards the end of the flight (after 10:15 UTC), measurements have been affected by aerosol or clouds, which resulted in increased filtering of data and reduced retrieval quality (see Supplement).

In horizontal-vertical space, the pollution gas distributions are strongly correlated pointing to self-consistent measurements. However, the highest VMRs for each trace gas are not always observed within the same air masses. For example, C_2H_6 shows

155 highest VMRs at the maximum at 8:00 UTC and 8 km altitude, but PAN, HCOOH, and CH_3OH have comparably low absolute VMRs for this local maximum. For C_2H_4, the species with the shortest atmospheric lifetime (see Tab. 1), only two maxima are observed, in contrast to many distinct maxima in the other species. This indicates that these air masses have been recently transported from a biomass burning source to the measurement location. A further investigation of the air mass origin will be presented in Sect. 4, based on the analysis of backward trajectories.

160 ## 3.2 Flight on 7 October 2019

The flight on 7 October 2019 was similar to the flight on 8 September 2019, but in the opposite direction. The flight was routed from Buenos Aires to Sal, and this time, GLORIA tangent points were directed eastwards, away from the South American coast (see Fig. 2a). Again, a large number of fires was reported by FIRMS above central South America. The horizontal winds show a strong westerly component at approximately 40°W, which may have transported polluted air from the fires to the measurement

165 locations.

Cross sections of the pollution trace gases for this flight are presented in Fig. 2b-f. Until 17:30 UTC, no considerable enhanced structure is observed for any discussed trace gas. Afterwards, a remarkable nose-shaped maximum is measured for PAN, C_2H_6, HCOOH, and CH_3OH between 17:30 UTC and 20:00 UTC, and 8 km to 13 km altitude (orange). Within this plume, maximum VMRs of PAN up to 1000 pptv, of C_2H_6 up to 1400 pptv, of HCOOH up to 500 pptv, and of CH_3OH up to

170 4500 pptv are observed. For C_2H_4, only a small enhancement at 19:30 UTC and 11 km altitude with VMRs up to 120 pptv is measured. These are the same air masses, for which PAN and CH_3OH have their highest VMRs within the larger plume. A smaller enhancement in all discussed trace gases is observed between 19:00 UTC and 21:00 UTC, above cloud top altitude, at 6 km (up to 800 pptv for PAN, 1100 pptv for C_2H_6, 800 pptv for HCOOH, 2500 pptv for CH_3OH, and 300 pptv for C_2H_4; cyan). However, these enhancements are affected by a considerably higher absolute total estimated error (see Supplement), and

175 therefore these measurements are not as reliable as others. Further, a smaller maximum is measured between 20:00 UTC and 21:00 UTC at 7.5 km altitude (magenta) for PAN (300 pptv), C_2H_6 (900 pptv), HCOOH (300 pptv), and CH_3OH (1500 pptv).

The ERA5 horizontal winds suggest that the largest plume observed during this flight was transported from fires in central South America. The relatively low measured VMRs for C_2H_4 indicate that the plume has been transported in the atmosphere for clearly more than a few days (the upper tropospheric lifetime of C_2H_4 is 1.2 days (see Tab. 1).
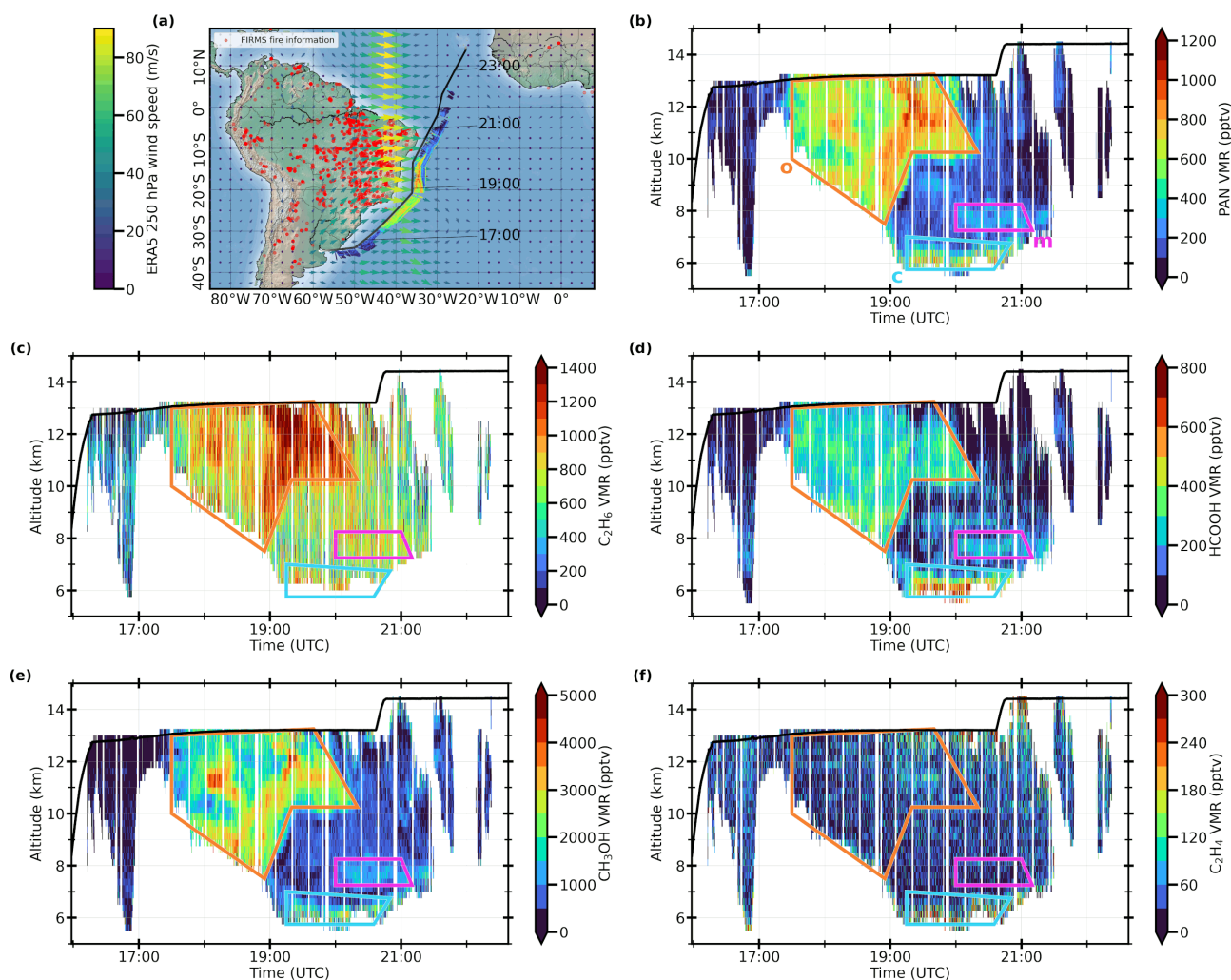
Figure 2. Same as Fig. 1, but for SouthTRAC flight on 7 October 2019 from Buenos Aires, Argentina to Sal, Cape Verde. In panel (a), ERA5 winds are displayed at 19:00 UTC. Note that colorbars may have changed compared to Fig. 1.

4 Trajectory analysis

For the geolocations (latitude, longitude, altitude, time) of the GLORIA measurements marked by colored boxes in the cross sections shown in Figs. 1-2 (colors are specified in Sect. 3), HYSPLIT seven day backward trajectories have been calculated and are presented in their horizontal evolution in Fig. 3. For a comparison with potential emission sources, additionally PAN surface VMRs of the CAMS model are shown as seven day averages for the time before each flight. These HYSPLIT backward trajectories are not expected to reasonably reproduce vertical motion of the air masses and therefore no vertical information is presented in the following figures. For the interpretation of the trajectories, this means that the origin of the examined air mass can be at any point along the backward trajectory connected with this particular air mass.
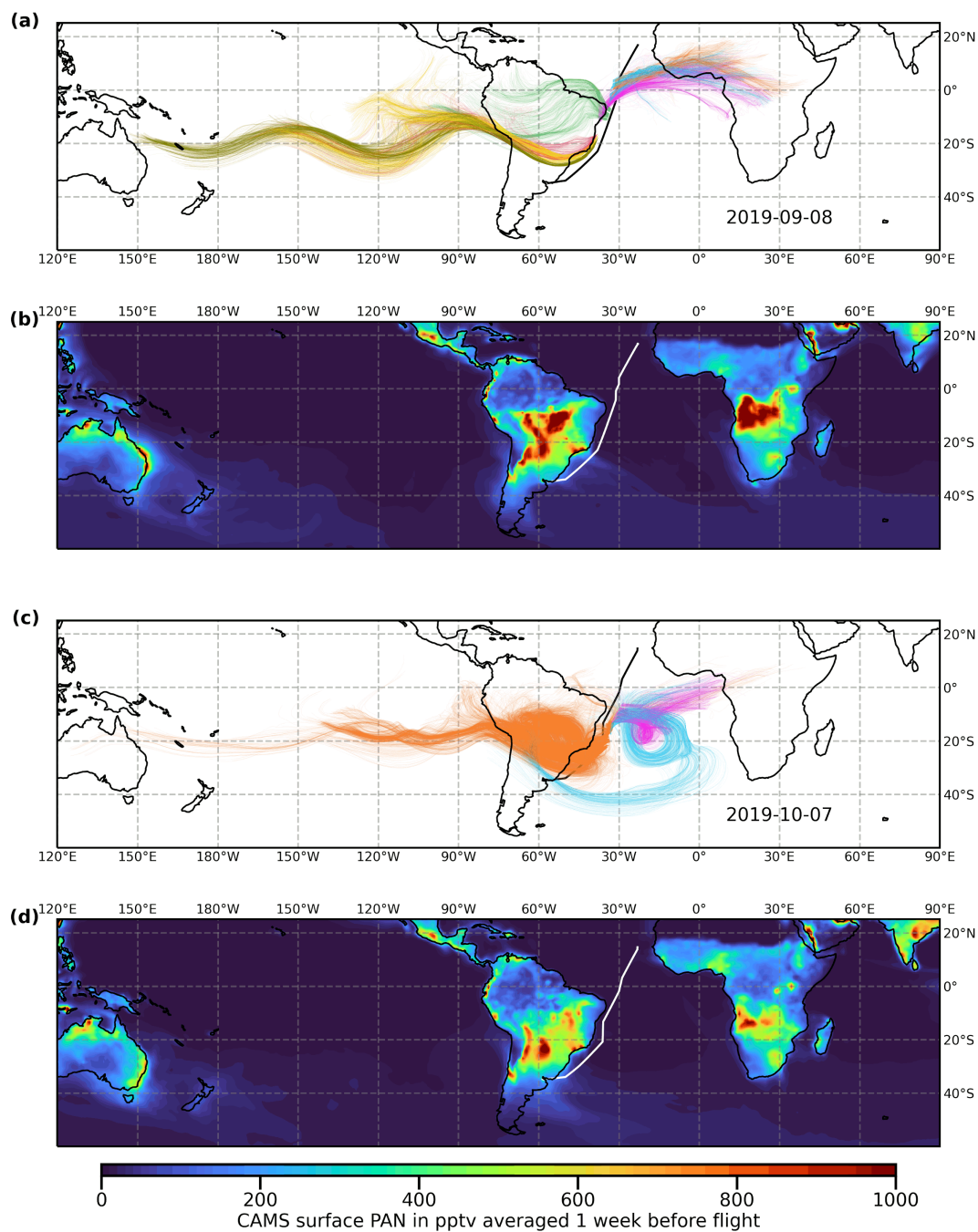
Figure 3. Horizontal evolution of HYSPLIT 7 days backward trajectories, starting at colored regions, as marked in Figs. 4-5 for flights on (a) 8 September 2019, and (c) 7 October 2019. Panels b and d show surface level volume mixing ratios of PAN, averaged over one week before the corresponding research flight, as reported by the CAMS model.

Trajectories for the flight on 8 September 2019 are shown in Fig. 3a. Because of the many small scale maximum structures in the measurements, trajectories from many different colored regions have been calculated. It can be seen that cyan, magenta, and

190 orange marked air masses come from central Africa, while green, red, yellow, and olive marked air masses come from South America. These different origins of air masses are also in agreement with the measured distributions of C_2H_4, the pollution trace gas with the shortest atmospheric lifetime in this study. This gas is only enhanced within the yellow and olive marked air masses, which both are indicated to come from South America. However, the red and green marked air masses also come from South America (according to the HYSPLIT trajectories), but do not show enhanced VMRs of C_2H_4. In particular, trajectories

195 for the red marked air masses look very similar to those marked yellow and olive. Possible reasons for these different C_2H_4 concentrations of air masses with similar origin may be different emissions of C_2H_4, higher loss processes for the different air masses, or different timing of vertical transport, which is not analyzed here. In Fig. 3b, CAMS surface PAN VMRs, averaged one week before the flight, can be compared to the trajectory paths. As expected from the FIRMS fire data shown in Fig. 1a, elevated PAN concentrations are present in central South America and central Africa. These are also the regions, where the

200 HYSPLIT backward trajectories indicate the origin of the measured polluted air masses.

For the flight on 7 October 2019, three air masses of interest have been marked by colored boxes in Fig. 2. The paths of backward trajectories connected with these air masses are shown in Fig. 3c. As discussed in the previous section, pollution trace gas measurements of this flight are dominated by a major plume, marked with an orange box. HYSPLIT backward trajectories starting from this orange marked plume indicate an origin of these air masses from the central South American continent. As

205 already estimated from the FIRMS fire data and ERA5 horizontal winds in Fig. 2a, it is likely that these polluted air masses come from biomass burning events in central South America. Surface concentrations of PAN (Fig. 3d), also illustrate enhanced PAN VMRs at this region. Air masses from smaller maxima during this flight, marked cyan and magenta, instead have been first transported longer paths above the South Atlantic. The pollution trace gases of the cyan marked air masses have been emitted in South America, and then been transported above the South Atlantic for approximately one week, before they reached the

210 measurement location. The backward trajectories associated with the magenta marked air masses also have been transported above the South Atlantic for one week before the measurement. Before this one week above the ocean, these air masses appear to come from central Africa, which is also a region of slightly enhanced PAN surface VMRs according to the CAMS model. These relatively lower enhancements of surface PAN are in agreement with the relatively lower enhancements of the GLORIA PAN VMRs.

215 **5 Comparison to CAMS model simulations**

In this section, GLORIA PAN, C_2H_6, HCOOH, CH_3OH, and C_2H_4 trace gas distributions will be used to evaluate CAMS model results. Figs. 4-5 present comparisons of these pollution trace gas measurements to CAMS simulation results, which have been temporally and spatially interpolated to the GLORIA tangent point locations and measurement times. In order to ensure a meaningful comparison, up to 27 GLORIA profiles are averaged horizontally to have a comparable horizontal
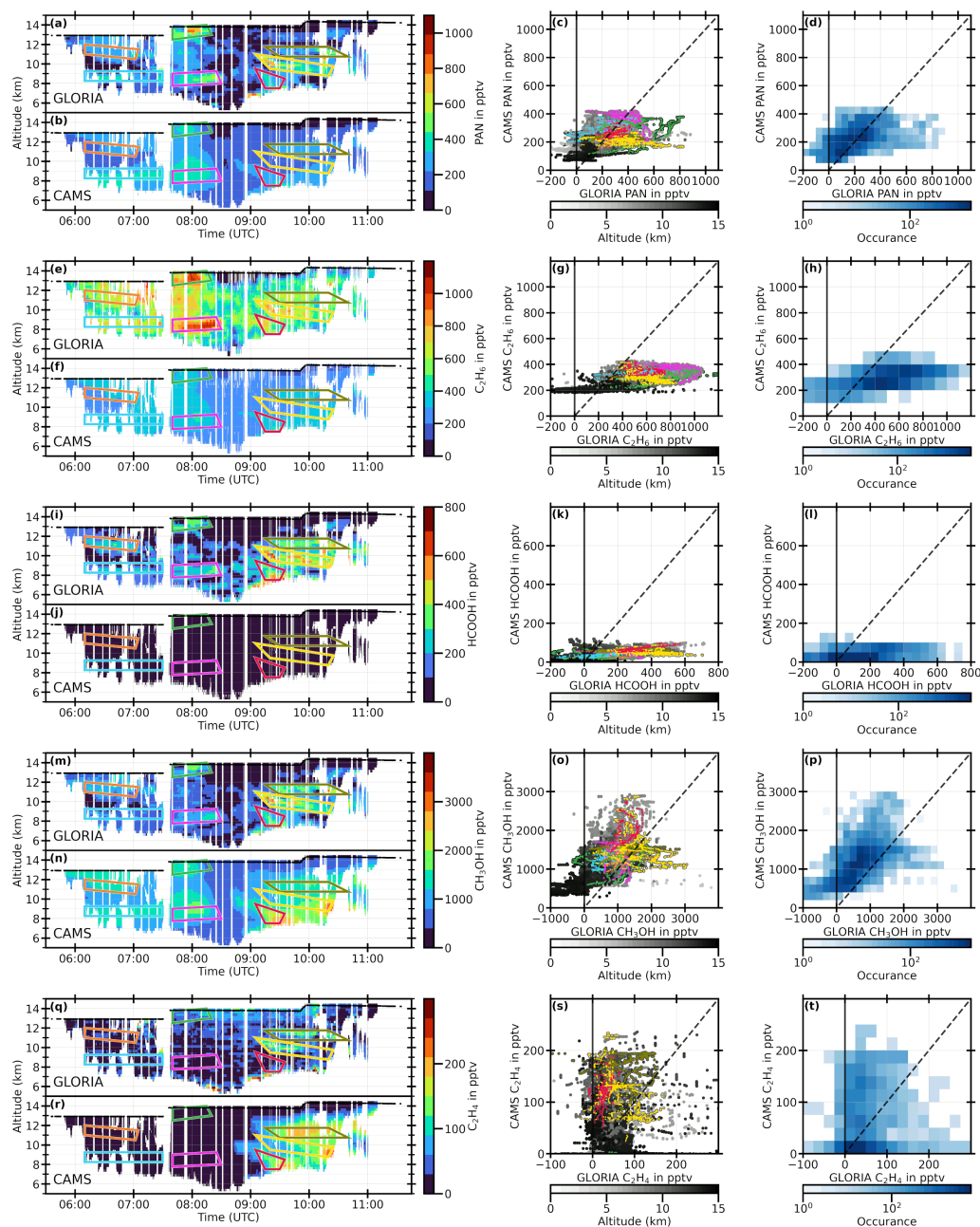
Figure 4. Comparison of GLORIA PAN (a-d), C_2H_6 (e-h), HCOOH (i-l), C_2H_4 (m-p), and CH_3OH (q-t) measurements to interpolated CAMS simulation results during SouthTRAC flight on 8 September 2019. In the left column, measurement and interpolated model results are compared as cross sections. Colored boxes mark regions with measurements of enhanced pollution trace gases and are repeated from Fig. 1. Panels in the second column show single point correlations, color coded by altitude, while panels on the right display the occurrence of these correlation points in fixed bins.

220 resolution to the CAMS model ($\approx$80 km). In these figures, first direct comparisons of measured and simulated pollution trace gas cross sections are shown, followed by correlation plots.

5.1 Flight on 8 September 2019

Figure 4 compares GLORIA measurements and CAMS simulation results for the research flight on 8 September 2019. For the direct comparison between distributions of PAN from GLORIA and CAMS (Fig. 4a-b), the model is able to reproduce

225 all measured structures that are marked with colored boxes, except for the air mass marked in yellow. In addition, absolute maximum PAN VMRs are simulated too low, in particular for the green marked air masses. The correlation plots reflect this overall agreement between measurement and model, within the estimated errors of the GLORIA retrieval (see Tab. 2). In the point-wise correlation plot (Fig. 4c), it is illustrated that points that are far away from the dashed line are connected with yellow and green marked air masses, which have been identified as problematic in the cross section comparison before. With help of

230 the histogram correlation plot (Fig. 4d) it is shown that the majority of correlation points is close to the dashed line (assuming a GLORIA total estimated error of up to 130 pptv).

In the direct comparison of C_2H_6 (Fig. 4e-f), some of the measured local maxima are reproduced by the model (e.g., red, magenta or green boxes), but overall C_2H_6 maxima and background values are simulated too low by the CAMS model. This underestimation of C_2H_6 by the model is also illustrated by the correlation plots (Fig. 4g-h). The comparison of measured and

235 simulated HCOOH is presented in Fig. 4i-l. While multiple enhancements up to 700 pptv are observed by GLORIA, CAMS simulates less than 100 pptv of HCOOH for the entire cross section.

In contrast to HCOOH, CAMS succeeds to reproduce the measured distribution of CH_3OH qualitatively, as it does for PAN and C_2H_6. Relative maxima (except the one of the yellow marked air mass) are represented by the model (Fig. 4m-n), and most of the absolute VMRs are in the same order of magnitude as the ones of the GLORIA measurements. However, background

240 VMRs are typically simulated too high. In the correlation plots (Fig. 4o-p), it is illustrated that overall the model overestimates CH_3OH concentrations, in particular for the red marked air masses. For the missing simulated local maximum at the yellow marked air masses, CAMS underestimates measured VMRs.

For C_2H_4 (Fig. 4q-r), only distinct local maxima are observed by GLORIA during the second part of the flight, at the olive and yellow marked air masses. CAMS also only simulates enhancements of C_2H_4 during the second part of the flight,

245 accordingly with the measurements. However, absolute C_2H_4 VMRs are simulated considerably higher than measured (typically 200 pptv compared to 150 pptv). In particular, the yellow marked air masses do not contain a simulated maximum, even though it was measured. In contrast, the red marked air masses have a simulated maximum, which was not measured. This overestimation is also shown in the correlation plots (Fig. 4s-t).

5.2 Flight on 7 October 2019

250 The flight on 7 October 2019 is characterized by a prominent nose-like plume. In Fig. 5a-b, the direct comparison of GLORIA and CAMS PAN is presented. The largest plume (marked with an orange box) is simulated by CAMS in quantitative agreement with the GLORIA measurements. A smaller measured local maximum structure above the cloud top (marked cyan), is also
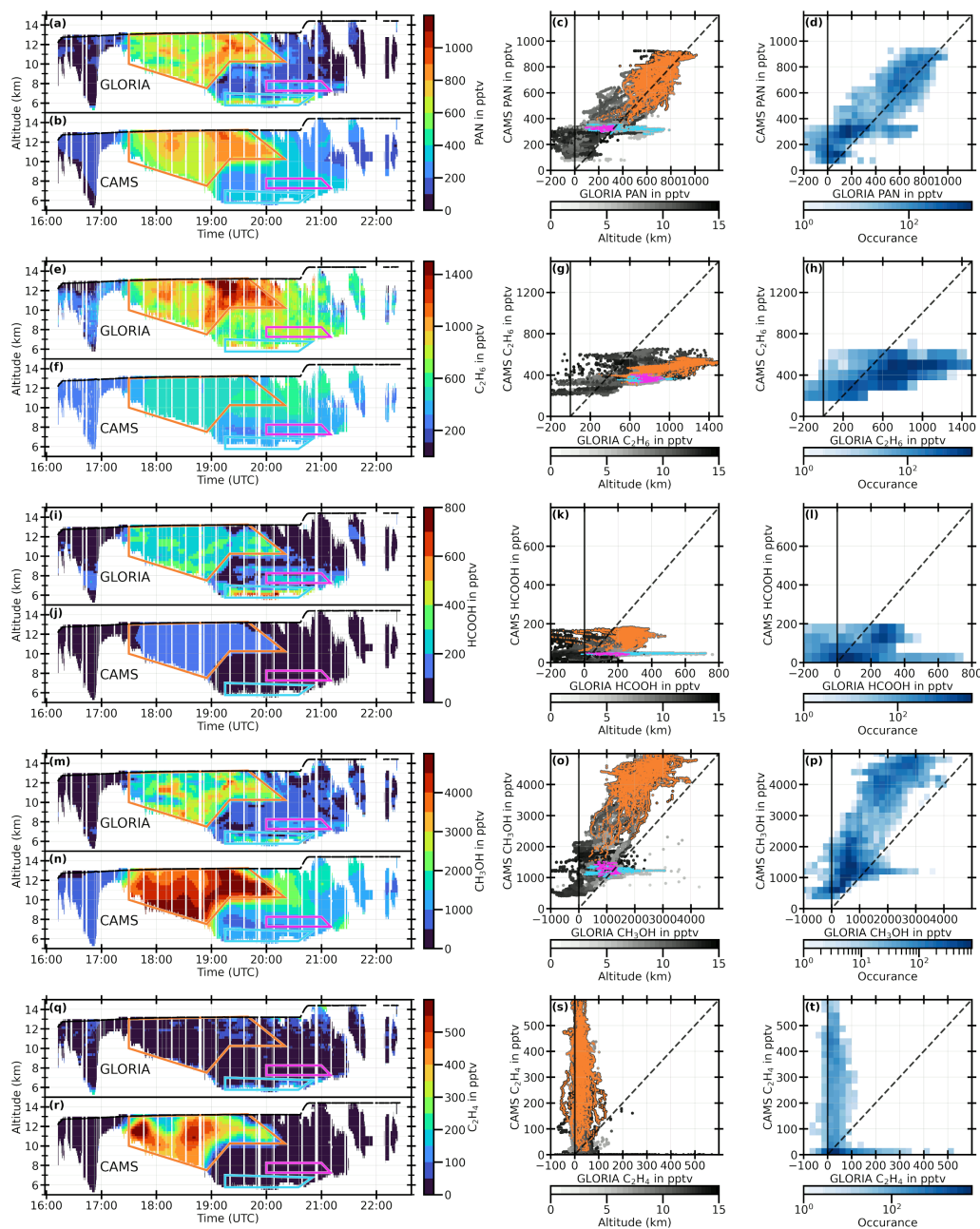
Figure 5. Same as Fig. 4, but for SouthTRAC flight on 7 October 2019. Note that colorbars may have changed compared to Fig. 4.

reproduced by CAMS, but with lower absolute VMRs (700 pptv measured compared to 300 pptv simulated). An even smaller measured local maximum (300 pptv) is marked by a magenta box. Although the absolute VMRs in this box are comparable in the simulation, this maximum is not distiguishable from the background VMRs, which are generally higher in the simulation

than in the measurement. The overall agreement between measurement and simulation is confirmed by the correlation plots (Fig. 5c-d). As discussed, lower simulated VMRs for the cyan marked air masses stand out, together with overall slightly higher simulated PAN background VMRs.

260 For C_2H_6 (Fig. 5e-f), also the major plume (orange) is clearly visible in the GLORIA measurement. However, for the simulation, the plume's shape is not easy to recognize. A smaller enhancement is simulated within the orange marked air masses, and increasing up to 600 pptv (compared to more than 1400 pptv measured) until the middle of the flight. Secondary maxima that have been measured (magenta and cyan) are not reproduced by the model. This overall underestimation of CAMS C_2H_6 is also illustrated by the correlation plots (Fig. 5g-h).

In Fig. 5i-j, comparisons of GLORIA and CAMS HCOOH are shown. The measurements again show the large plume 265 (orange, up to 500 pptv) and a large enhancement of smaller extent above cloud top altitude (cyan, up to 800 pptv) and above (magenta, up to 300 pptv). However, CAMS is only able to reproduce the orange marked plume with considerably too low absolute VMRs below 200 pptv of HCOOH, while the cyan and magenta maxima are not reproduced at all. This underestimation of simulated HCOOH of the orange marked plume, and for the cyan marked air masses in particular is also visible in the correlation plots (Fig. 5k-l).

270 In contrast to C_2H_6 and HCOOH, CH_3OH is overestimated by the CAMS model (Fig. 5m-n). The major plume (orange) is measured with up to 4000 pptv, while CAMS simulation results show more than 5000 pptv of CH_3OH. Secondary maxima (cyan and magenta) are measured for CH_3OH, but cannot be distinguished from the generally too high background of the simulation results. This is also reflected by the correlation plots (Fig. 5o-p), where the overall overestimation of CH_3OH is illustrated, in particular for the orange marked plume. The cyan marked air masses are, however, slightly underestimated by 275 CAMS.

For C_2H_4, only a tiny enhancement of less than 120 pptv is measured by GLORIA within the orange marked plume. In contrast, CAMS shows large enhancements of up to more than 600 pptv of C_2H_4 over the whole orange marked air masses (Fig. 5q-r). This overall overestimation is also reflected in the correlation plots (Fig. 5s-t).

5.3 Discussion

280 The comparisons between measured GLORIA pollution trace gas cross sections and CAMS simulation results show that CAMS is able to reproduce observed major plume structures. For PAN, absolute VMRs reveal a reasonable agreement, while C_2H_6 and HCOOH are underestimated, and CH_3OH and C_2H_4 are overestimated by the model. The overall agreement for PAN in space and time even for most of the small scale structures measured during the flight on 8 September 2019 indicates the ability of the CAMS model to correctly transport the polluted air masses from reasonably assumed emission sources within the 285 model. This strength of the CAMS model to reproduce structures of pollution trace gases correctly is also demonstrated in the comparison of the flight on 7 October 2019.

The underestimation of C_2H_6 and HCOOH, and the overestimation of CH_3OH and C_2H_4 may have several reasons: The composition of polluted air masses is difficult to estimate, leading to possibly erroneous trace gas emissions used by the model (Flemming et al., 2015), and atmospheric lifetimes may be influenced by uncertain or incomplete reaction properties of source

290 and loss processes within the model. For HCOOH, it is known that a common model shortcut (transforming formaldehyde into HCOOH inside clouds without considering methanediol as intermediate) causes a too high washout of HCOOH and overall too low HCOOH concentrations (Franco et al., 2021).

6 Conclusions

This study discusses simultaneous airborne measurements of PAN, C_2H_6, HCOOH, CH_3OH, and C_2H_4 measured by GLORIA
295 during the SouthTRAC campaign in September and October 2019. Both discussed research flights have been performed above the South Atlantic, and revealed different two dimensional vertically resolved distributions of the discussed pollution trace gases. While the flight on 8 September 2019 revealed a filamentary structure of pollution trace gas enhancements, the flight on 7 October 2019 was characterized by a large plume with high absolute VMRs of all discussed trace gases but C_2H_4. For each flight, two dimensional distributions of the discussed trace gases are coherent, considering the different atmospheric lifetimes,
300 showing the good quality of the GLORIA retrieval.

The analysis of the horizontal components of HYSPLIT backward trajectories starting at GLORIA measurement geolocations with enhanced pollution trace gas VMRs illustrated the South American and African origin of the upper tropospheric air masses above the South Atlantic. While during the flight on 8 September 2019 polluted air masses showed a filamentary structure and came from both, South America and central Africa, the second flight discussed was characterized by a major
305 plume, coming from central South America. Smaller polluted air masses measured during that flight have traveled above the South Atlantic for approximately one week, after they have been released either from South America or Africa. This trajectory analysis also helps to explain the enhancements of C_2H_4, which only were observed for some of the peaks of the other measured pollution trace gases. From the trajectory analysis, it is confirmed that these air masses with the shorter lived substance C_2H_4 enhanced, have been recently released in South America and have not traveled for long distances.

310 The comparison of the GLORIA cross sections with interpolated CAMS reanalysis data illustrates the strength of the CAMS model to reproduce measured PAN VMR distributions. For PAN, structures and absolute VMRs are repeated by the model as expected for the given model resolution. This is in line with results from Wang et al. (2020) for the northern hemisphere. Structures of CAMS C_2H_6 are overall in agreement with GLORIA for both discussed research flights, but absolute VMRs are underestimated, which has been also observed in the northern hemisphere by Wang et al. (2020). HCOOH is also largely
315 underestimated by CAMS, which has been observed by Wetzel et al. (2021) in the northern hemisphere, too. During the flight on 8 September 2019, enhancements of the model HCOOH data are so low that it is not possible to distinguish those from typical background VMRs. Simulations for the flight on 7 October 2019 are able to reproduce the large plume of HCOOH qualitatively, but with considerably too low absolute VMRs. As discussed, this underestimation of HCOOH by the model is possibly caused by a shortcut of HCOOH chemistry in clouds (see Franco et al., 2021). CH_3OH instead is overestimated by
320 the model, for both, peak and background VMRs. Structures measured by GLORIA are, however, reproduced by CAMS. For C_2H_4, CAMS is able to simulate the measured filaments of the flight on 8 September 2019, but overestimates the absolute VMR and shows an enhancement at air masses that do not have observed elevated VRMs. CAMS correctly shows no enhancement

of C_2H_4 for parts of the flight, where GLORIA measurements do not indicate enhancements. This is in contrast to the flight on 7 October 2019, where CAMS showed strong enhancements within the large plume, that has been measured for all trace gases

325 but C_2H_4. Overall, CAMS also overestimates absolute VMRs of C_2H_4.

In summary, we find that PAN is simulated remarkably well by the model, and that for the other discussed trace gases measured structures are overall reproduced. This indicates that the location of the emission sources and the atmospheric dynamics of the CAMS model perform well. For PAN, also emission strengths of precursor gases, and atmospheric gain and loss processes of the model are able to reproduce observed distributions that quantitatively compare with the GLORIA measurements.

330 However, for the other discussed pollution trace gases, absolute VMRs are not in agreement with the GLORIA observations. It is suggested that emissions strengths and atmospheric source and loss processes should be improved in CAMS for these species. In particular, for HCOOH, known problems should be avoided by not using the common model shortcut. Our comparison with CAMS shows the strength of high resolution altitude resolved measurements of multiple species in order to find strengths and deficiencies of atmospheric models.

335 *Data availability.* GLORIA measurements are available in the database HALO-DB (https://halo-db.pa.op.dlr.de/mission/116) and will be available on the KITopen repository. The CAMS model data is available from the Copernicus Atmosphere Data Store (https://ads.atmosphere. copernicus.eu).

Author contributions. SJ initiated the study, performed the analyses, and wrote the manuscript. GW, MH, JU, AK, NG, and SJ performed the GLORIA data processing. FFV, TN and coworkers operated GLORIA during the SouthTRAC campaign. BMS and coworkers coordinated
340 the SouthTRAC campaign. All authors commented on and improved the manuscript.

Competing interests. The authors declare that they have no conflict of interest.

Acknowledgements. We gratefully thank the SouthTRAC coordination team, in particular DLR-FX for successfully conducting the field campaign. The results are based on the efforts of all members of the GLORIA team, including the technology institutes ZEA-1 and ZEA-2 at Forschungszentrum Jülich and the Institute for Data Processing and Electronics at the Karlsruhe Institute of Technology. We thank
345 ECMWF for providing CAMS data. The authors acknowledge the NOAA Air Resources Laboratory (ARL) for the provision of the HYSPLIT transport and dispersion model used in this publication. We acknowledge support by the German Research Foundation (Deutsche Forschungsgemeinschaft, DFG Priority Program SPP 1294). We further acknowledge support by the KIT-Publication Fund of the Karlsruhe Institute of Technology.

References

350 Abram, N. J., Henley, B. J., Sen Gupta, A., Lippmann, T. J. R., Clarke, H., Dowdy, A. J., Sharples, J. J., Nolan, R. H., Zhang, T., Wooster, M. J., Wurtzel, J. B., Meissner, K. J., Pitman, A. J., Ukkola, A. M., Murphy, B. P., Tapper, N. J., and Boer, M. M.: Connections of climate change and variability to large and extreme forest fires in southeast Australia, Communications Earth & Environment, 2, 1–17, https://doi.org/10.1038/s43247-020-00065-8, https://www.nature.com/articles/s43247-020-00065-8, 2021.

Andreae, M. O. and Merlet, P.: Emission of trace gases and aerosols from biomass burning, Global Biogeochemical Cycles, 15, 955–966,
355 https://doi.org/10.1029/2000GB001382, 2001.

Bates, K. H., Jacob, D. J., Wang, S., Hornbrook, R. S., Apel, E. C., Kim, M. J., Millet, D. B., Wells, K. C., Chen, X., Brewer, J. F., Ray, E. A., Commane, R., Diskin, G. S., and Wofsy, S. C.: The Global Budget of Atmospheric Methanol: New Constraints on Secondary, Oceanic, and Terrestrial Sources, Journal of Geophysical Research: Atmospheres, 126, e2020JD033 439, https://doi.org/10.1029/2020JD033439, https://agupubs.onlinelibrary.wiley.com/doi/full/10.1029/2020JD033439, 2021.

360 Coheur, P.-F., Herbin, H., Clerbaux, C., Hurtmans, D., Wespes, C., Carleer, M., Turquety, S., Rinsland, C. P., Remedios, J., Hauglustaine, D., Boone, C. D., and Bernath, P. F.: ACE-FTS observation of a young biomass burning plume: First reported measurements of C_2H_4, C_3H_6O, H_2CO and PAN by infrared occultation from space, Atmospheric Chemistry and Physics, 7, 5437–5446, https://doi.org/10.5194/acp-7-5437-2007, https://www.atmos-chem-phys.net/7/5437/2007/acp-7-5437-2007.pdf, 2007.

Coheur, P.-F., Clarisse, L., Turquety, S., Hurtmans, D., and Clerbaux, C.: IASI measurements of reactive trace species in biomass burning
365 plumes, Atmospheric Chemistry and Physics, 9, 5655–5667, https://doi.org/10.5194/acp-9-5655-2009, https://www.atmos-chem-phys.net/9/5655/2009/acp-9-5655-2009.pdf, 2009.

Dolan, W., Payne, V. H., Kualwik, S. S., and Bowman, K. W.: Satellite observations of ethylene (C_2H_4) from the Aura Tropospheric Emission Spectrometer: A scoping study, Atmospheric Environment, 141, 388–393, https://doi.org/10.1016/j.atmosenv.2016.07.009, http://www.sciencedirect.com/science/article/pii/S1352231016305283, 2016.

370 Dufour, G., Szopa, S., Hauglustaine, D. A., Boone, C. D., Rinsland, C. P., and Bernath, P. F.: The influence of biogenic emissions on upper-tropospheric methanol as revealed from space, Atmospheric Chemistry and Physics, 7, 6119–6129, https://doi.org/10.5194/acp-7-6119-2007, 2007.

Fischer, E. V., Jacob, D. J., Yantosca, R. M., Sulprizio, M. P., Millet, D. B., Mao, J., Paulot, F., Singh, H. B., Roiger, A., Ries, L., Talbot, R. W., Dzepina, K., and Pandey Deolal, S.: Atmospheric peroxyacetyl nitrate (PAN): A global budget and source attribution, Atmo-
375 spheric Chemistry and Physics, 14, 2679–2698, https://doi.org/10.5194/acp-14-2679-2014, https://www.atmos-chem-phys.net/14/2679/2014/acp-14-2679-2014.pdf, 2014.

Flemming, J., Huijnen, V., Arteta, J., Bechtold, P., Beljaars, A., Blechschmidt, A.-M., Diamantakis, M., Engelen, R. J., Gaudel, A., Inness, A., Jones, L., Josse, B., Katragkou, E., Marecal, V., Peuch, V.-H., Richter, A., Schultz, M. G., Stein, O., and Tsikerdekis, A.: Tropospheric chemistry in the Integrated Forecasting System of ECMWF, Geoscientific Model Development, 8, 975–1003, https://doi.org/10.5194/gmd-
380 8-975-2015, https://www.geosci-model-dev.net/8/975/2015/gmd-8-975-2015.pdf, 2015.

Franco, B., Clarisse, L., Stavrakou, T., Müller, J., van Damme, M., Whitburn, S., Hadji-Lazaro, J., Hurtmans, D., Taraborrelli, D., Clerbaux, C., and Coheur, P.: A General Framework for Global Retrievals of Trace Gases From IASI: Application to Methanol, Formic Acid, and PAN, Journal of Geophysical Research: Atmospheres, 123, 13,963–13,984, https://doi.org/10.1029/2018JD029633, https://agupubs.onlinelibrary.wiley.com/doi/full/10.1029/2018JD029633, 2018.

385   Franco, B., Blumenstock, T., Cho, C., Clarisse, L., Clerbaux, C., Coheur, P.-F., Mazière, M. D., de Smedt, I., Dorn, H.-P., Emmerichs, T., Fuchs, H., Gkatzelis, G., Griffith, D. W. T., Gromov, S., Hannigan, J. W., Hase, F., Hohaus, T., Jones, N., Kerkweg, A., Kiendler-Scharr, A., Lutsch, E., Mahieu, E., Novelli, A., Ortega, I., Paton-Walsh, C., Pommier, M., Pozzer, A., Reimer, D., Rosanka, S., Sander, R., Schneider, M., Strong, K., Tillmann, R., van Roozendael, M., Vereecken, L., Vigouroux, C., Wahner, A., and Taraborrelli, D.: Ubiquitous atmospheric production of organic acids mediated by cloud droplets, Nature, 593, 233–237, https://doi.org/10.1038/s41586-021-03462-x,

390   https://www.nature.com/articles/s41586-021-03462-x, 2021.

Friedl-Vallon, F., Gulde, T., Hase, F., Kleinert, A., Kulessa, T., Maucher, G., Neubert, T., Olschewski, F., Piesch, C., Preusse, P., Rongen, H., Sartorius, C., Schneider, H., Schönfeld, A., Tan, V., Bayer, N., Blank, J., Dapp, R., Ebersoldt, A., Fischer, H., Graf, F., Guggenmoser, T., Höpfner, M., Kaufmann, M., Kretschmer, E., Latzko, T., Nordmeyer, H., Oelhaf, H., Orphal, J., Riese, M., Schardt, G., Schillings, J., Sha, M. K., Suminska-Ebersoldt, O., and Ungermann, J.: Instrument concept of the imaging Fourier transform spectrometer GLORIA,

395   Atmospheric Measurement Techniques, 7, 3565–3577, https://doi.org/10.5194/amt-7-3565-2014, 2014.

Gettelman, A., Hoor, P., Pan, L. L., Randel, W. J., Hegglin, M. I., and Birner, T.: The extratropical Upper Troposphere and Lower Stratosphere, Reviews of Geophysics, 49, 2011RG000 355, https://doi.org/10.1029/2011RG000355, 2011.

Glatthor, N., von Clarmann, T., Fischer, H., Funke, B., Grabowski, U., Höpfner, M., Kellmann, S., Kiefer, M., Linden, A., Milz, M., Steck, T., and Stiller, G. P.: Global peroxyacetyl nitrate (PAN) retrieval in the upper troposphere from limb emission spectra of the Michelson Inter-

400   ferometer for Passive Atmospheric Sounding (MIPAS), Atmospheric Chemistry and Physics, 7, 2775–2787, https://doi.org/10.5194/acp-7-2775-2007, https://www.atmos-chem-phys.net/7/2775/2007/acp-7-2775-2007.pdf, 2007.

Glatthor, N., Höpfner, M., Stiller, G. P., von Clarmann, T., Funke, B., Lossow, S., Eckert, E., Grabowski, U., Kellmann, S., Linden, A., A. Walker, K., and Wiegele, A.: Seasonal and interannual variations in HCN amounts in the upper troposphere and lower stratosphere observed by MIPAS, Atmospheric Chemistry and Physics, 15, 563–582, https://doi.org/10.5194/acp-15-563-2015, 2015.

405   Gordon, I. E., Rothman, L. S., Hill, C., Kochanov, R. V., Tan, Y., Bernath, P. F., Birk, M., Boudon, V., Campargue, A., Chance, K. V., Drouin, B. J., Flaud, J. M., Gamache, R. R., Hodges, J. T., Jacquemart, D., Perevalov, V. I., Perrin, A., Shine, K. P., Smith, M. A. H., Tennyson, J., Toon, G. C., Tran, H., Tyuterev, V. G., Barbe, A., Császár, A. G., Devi, V. M., Furtenbacher, T., Harrison, J. J., Hartmann, J. M., Jolly, A., Johnson, T. J., Karman, T., Kleiner, I., Kyuberis, A. A., Loos, J., Lyulin, O. M., Massie, S. T., Mikhailenko, S. N., Moazzen-Ahmadi, N., Müller, H. S. P., Naumenko, O. V., Nikitin, A. V., Polyansky, O. L., Rey, M., Rotger, M., Sharpe, S. W., Sung, K., Starikova, E.,

410   Tashkun, S. A., Auwera, J. V., Wagner, G., Wilzewski, J., Wcisło, P., Yu, S., and Zak, E. J.: The HITRAN2016 molecular spectroscopic database, Journal of Quantitative Spectroscopy and Radiative Transfer, 203, 3–69, https://doi.org/10.1016/j.jqsrt.2017.06.038, http://www.sciencedirect.com/science/article/pii/S0022407317301073, 2017.

Granier, C., Bessagnet, B., Bond, T., D'Angiola, A., van der Denier Gon, H., Frost, G. J., Heil, A., Kaiser, J. W., Kinne, S., Klimont, Z., Kloster, S., Lamarque, J.-F., Liousse, C., Masui, T., Meleux, F., Mieville, A., Ohara, T., Raut, J.-C., Riahi, K., Schultz, M. G., Smith, S. J.,

415   Thompson, A., van Aardenne, J., van der Werf, G. R., and van Vuuren, D. P.: Evolution of anthropogenic and biomass burning emissions of air pollutants at global and regional scales during the 1980–2010 period, Climatic Change, 109, 163–190, https://doi.org/10.1007/s10584-011-0154-1, 2011.

Grutter, M., Glatthor, N., Stiller, G. P., Fischer, H., Grabowski, U., Höpfner, M., Kellmann, S., Linden, A., and von Clarmann, T.: Global distribution and variability of formic acid as observed by MIPAS-ENVISAT, Journal of Geophysical Research: Atmospheres, 115,

420   https://doi.org/10.1029/2009JD012980, https://agupubs.onlinelibrary.wiley.com/doi/full/10.1029/2009JD012980, 2010.

Guenther, A. B., Jiang, X., Heald, C. L., Sakulyanontvittaya, T., Duhl, T., Emmons, L. K., and Wang, X.: The Model of Emissions of Gases and Aerosols from Nature version 2.1 (MEGAN2.1): an extended and updated framework for modeling biogenic emissions, Geoscientific Model Development, 5, 1471–1492, https://doi.org/10.5194/gmd-5-1471-2012, https://gmd.copernicus.org/articles/5/1471/2012/, 2012.

425 Guggenmoser, T., Blank, J., Kleinert, A., Latzko, T., Ungermann, J., Friedl-Vallon, F., Höpfner, M., Kaufmann, M., Kretschmer, E., Maucher, G., Neubert, T., Oelhaf, H., Preusse, P., Riese, M., Rongen, H., Sha, M. K., Sumińska-Ebersoldt, O., and Tan, V.: New calibration noise suppression techniques for the GLORIA limb imager, Atmospheric Measurement Techniques, 8, 3147–3161, https://doi.org/10.5194/amt-8-3147-2015, https://www.atmos-meas-tech.net/8/3147/2015/amt-8-3147-2015.pdf, 2015.

Hoyle, C. R., Marécal, V., Russo, M. R., Allen, G., Arteta, J., Chemel, C., Chipperfield, M. P., D'Amato, F., Dessens, O., Feng, W., Hamilton, J. F., Harris, N. R. P., Hosking, J. S., Lewis, A. C., Morgenstern, O., Peter, T., Pyle, J. A., Reddmann, T., Richards, N. A. D., Telford, 430 P. J., Tian, W., Viciani, S., Volz-Thomas, A., Wild, O., Yang, X., and Zeng, G.: Representation of tropical deep convection in atmospheric models – Part 2: Tracer transport, Atmospheric Chemistry and Physics, 11, 8103–8131, https://doi.org/10.5194/acp-11-8103-2011, 2011.

Höpfner, M., Ungermann, J., Borrmann, S., Wagner, R., Spang, R., Riese, M., Stiller, G., Appel, O., Batenburg, A. M., Bucci, S., Cairo, F., Dragoneas, A., Friedl-Vallon, F., Hünig, A., Johansson, S., Krasauskas, L., Legras, B., Leisner, T., Mahnke, C., Möhler, O., Molleker, S., Müller, R., Neubert, T., Orphal, J., Preusse, P., Rex, M., Saathoff, H., Stroh, F., Weigel, R., and Wohltmann, I.: Ammonium ni-435 trate particles formed in upper troposphere from ground ammonia sources during Asian monsoons, Nature Geoscience, 12, 608–612, https://doi.org/10.1038/s41561-019-0385-8, 2019.

Inness, A., Flemming, J., Heue, K.-P., Lerot, C., Loyola, D., Ribas, R., Valks, P., van Roozendael, M., Xu, J., and Zimmer, W.: Monitoring and assimilation tests with TROPOMI data in the CAMS system: Near-real-time total column ozone, Atmospheric Chemistry and Physics, 19, 3939–3962, https://doi.org/10.5194/acp-19-3939-2019, https://www.atmos-chem-phys.net/19/3939/2019/acp-19-3939-2019.pdf, 2019.

440 Johansson, S., Woiwode, W., Höpfner, M., Friedl-Vallon, F., Kleinert, A., Kretschmer, E., Latzko, T., Orphal, J., Preusse, P., Ungermann, J., Santee, M. L., Jurkat-Witschas, T., Marsing, A., Voigt, C., Giez, A., Krämer, M., Rolf, C., Zahn, A., Engel, A., Sinnhuber, B.-M., and Oelhaf, H.: Airborne limb-imaging measurements of temperature, HNO_3, O_3, $ClONO_2$, H_2O and CFC-12 during the Arctic winter 2015/2016: Characterization, in situ validation and comparison to Aura/MLS, Atmospheric Measurement Techniques, 11, 4737–4756, https://doi.org/10.5194/amt-11-4737-2018, https://www.atmos-meas-tech.net/11/4737/2018/amt-11-4737-2018.pdf, 2018.

445 Johansson, S., Höpfner, M., Kirner, O., Wohltmann, I., Bucci, S., Legras, B., Friedl-Vallon, F., Glatthor, N., Kretschmer, E., Ungermann, J., and Wetzel, G.: Pollution trace gas distributions and their transport in the Asian monsoon upper troposphere and lowermost stratosphere during the StratoClim campaign 2017, Atmospheric Chemistry and Physics, 20, 14 695–14 715, https://doi.org/10.5194/acp-20-14695-2020, https://acp.copernicus.org/articles/20/14695/2020/acp-20-14695-2020.html, 2020.

Kaiser, J. W., Heil, A., Andreae, M. O., Benedetti, A., Chubarova, N., Jones, L., Morcrette, J.-J., Razinger, M., Schultz, M. G., Suttie, M., 450 and van der Werf, G. R.: Biomass burning emissions estimated with a global fire assimilation system based on observed fire radiative power, Biogeosciences, 9, 527–554, https://doi.org/10.5194/bg-9-527-2012, https://bg.copernicus.org/articles/9/527/2012/, 2012.

Khaykin, S., Legras, B., Bucci, S., Sellitto, P., Isaksen, L., Tencé, F., Bekki, S., Bourassa, A., Rieger, L., Zawada, D., Jumelet, J., and Godin-Beekmann, S.: The 2019/20 Australian wildfires generated a persistent smoke-charged vortex rising up to 35 km altitude, Communications Earth & Environment, 1, 1–12, https://doi.org/10.1038/s43247-020-00022-5, https://www.nature.com/articles/s43247-020-00022-5, 455 2020.

Kleinert, A., Friedl-Vallon, F., Guggenmoser, T., Höpfner, M., Neubert, T., Ribalda, R., Sha, M. K., Ungermann, J., Blank, J., Ebersoldt, A., Kretschmer, E., Latzko, T., Oelhaf, H., Olschewski, F., and Preusse, P.: Level 0 to 1 processing of the imaging Fourier transform

spectrometer GLORIA: Generation of radiometrically and spectrally calibrated spectra, Atmospheric Measurement Techniques, 7, 4167–4184, https://doi.org/10.5194/amt-7-4167-2014, 2014.

460   Lim, C. Y., Hagan, D. H., Coggon, M. M., Koss, A. R., Sekimoto, K., de Gouw, J., Warneke, C., Cappa, C. D., and Kroll, J. H.: Secondary organic aerosol formation from the laboratory oxidation of biomass burning emissions, Atmospheric Chemistry and Physics, 19, 12 797–12 809, https://doi.org/10.5194/acp-19-12797-2019, https://acp.copernicus.org/articles/19/12797/2019/acp-19-12797-2019.html, 2019.

Mauzerall, D. L., Logan, J. A., Jacob, D. J., Anderson, B. E., Blake, D. R., Bradshaw, J. D., Heikes, B., Sachse, G. W., Singh, H., and Talbot, B.: Photochemistry in biomass burning plumes and implications for tropospheric ozone over the tropical South Atlantic, Journal
465   of Geophysical Research, 103, 8401–8423, https://doi.org/10.1029/97JD02612, 1998.

Millet, D. B., Baasandorj, M., Farmer, D. K., Thornton, J. A., Baumann, K., Brophy, P., Chaliyakunnel, S., Gouw, J. A. d., Graus, M., Hu, L., Koss, A., Lee, B. H., Lopez-Hilfiker, F. D., Neuman, J. A., Paulot, F., Peischl, J., Pollack, I. B., Ryerson, T. B., Warneke, C., Williams, B. J., and Xu, J.: A large and ubiquitous source of atmospheric formic acid, Atmospheric Chemistry and Physics, 15, 6283–6304, https://doi.org/10.5194/acp-15-6283-2015, https://www.atmos-chem-phys.net/15/6283/2015/acp-15-6283-2015.pdf, 2015.

470   Morcrette, J., Boucher, O., Jones, L., Salmond, D., Bechtold, P., Beljaars, A., Benedetti, A., Bonet, A., Kaiser, J. W., Razinger, M., Schulz, M., Serrar, S., Simmons, A. J., Sofiev, M., Suttie, M., Tompkins, A. M., and Untch, A.: Aerosol analysis and forecast in the European Centre for Medium-Range Weather Forecasts Integrated Forecast System: Forward modeling, Journal of Geophysical Research: Atmospheres, 114, https://doi.org/10.1029/2008JD011235, https://agupubs.onlinelibrary.wiley.com/doi/pdf/10.1029/2008JD011235, 2009.

Morgott, D. A.: Anthropogenic and biogenic sources of Ethylene and the potential for human exposure: A literature review,
475   Chemico-Biological Interactions, 241, 10–22, https://doi.org/10.1016/j.cbi.2015.08.012, https://www.sciencedirect.com/science/article/pii/S0009279715002835, 2015.

Mungall, E. L., Abbatt, J. P. D., Wentzell, J. J. B., Wentworth, G. R., Murphy, J. G., Kunkel, D., Gute, E., Tarasick, D. W., Sharma, S., Cox, C. J., Uttal, T., and Liggio, J.: High gas-phase mixing ratios of formic and acetic acid in the High Arctic, Atmospheric Chemistry and Physics, 18, 10 237–10 254, https://doi.org/10.5194/acp-18-10237-2018, https://www.atmos-chem-phys.net/18/10237/
480   2018/acp-18-10237-2018.pdf, 2018.

Oelhaf, H., Sinnhuber, B.-M., Woiwode, W., Bönisch, H., Bozem, H., Engel, A., Fix, A., Friedl-Vallon, F., Grooß, J.-U., Hoor, P., Johansson, S., Jurkat-Witschas, T., Kaufmann, S., Krämer, M., Krause, J., Kretschmer, E., Lörks, D., Marsing, A., Orphal, J., Pfeilsticker, K., Pitts, M., Poole, L., Preusse, P., Rapp, M., Riese, M., Rolf, C., Ungermann, J., Voigt, C., Volk, C. M., Wirth, M., Zahn, A., and Ziereis, H.: Polstracc: Airborne Experiment for Studying the Polar Stratosphere in a Changing Climate with the High Altitude and Long Range Research Aircraft
485   (HALO), Bulletin of the American Meteorological Society, 100, 2634–2664, https://doi.org/10.1175/BAMS-D-18-0181.1, 2019.

Paulot, F., Wunch, D., Crounse, J. D., Toon, G. C., Millet, D. B., DeCarlo, P. F., Vigouroux, C., Deutscher, N. M., González Abad, G., Notholt, J., Warneke, T., Hannigan, J. W., Warneke, C., Gouw, J. A. d., Dunlea, E. J., Mazière, M. D., Griffith, D. W. T., Bernath, P., Jimenez, J. L., and Wennberg, P. O.: Importance of secondary sources in the atmospheric budgets of formic and acetic acids, Atmospheric Chemistry and Physics, 11, 1989–2013, https://doi.org/10.5194/acp-11-1989-2011, https://www.atmos-chem-phys.net/11/1989/
490   2011/acp-11-1989-2011.pdf, 2011.

Peischl, J., Eilerman, S. J., Neuman, J. A., Aikin, K. C., de Gouw, J., Gilman, J. B., Herndon, S. C., Nadkarni, R., Trainer, M., Warneke, C., and Ryerson, T. B.: Quantifying Methane and Ethane Emissions to the Atmosphere From Central and Western U.S. Oil and Natural Gas Production Regions, Journal of Geophysical Research: Atmospheres, https://doi.org/10.1029/2018JD028622, 2018.

Pope, R. J., Kerridge, B. J., Siddans, R., Latter, B. G., Chipperfield, M. P., Arnold, S. R., Ventress, L. J., Pimlott, M. A., Graham, A. M.,

495   Knappett, D. S., and Rigby, R.: Large enhancements in southern hemisphere satellite-observed trace gases due to the 2019/2020 Australian wildfires, Journal of Geophysical Research: Atmospheres, https://doi.org/10.1029/2021JD034892, 2021.

Rapp, M., Kaifler, B., Dörnbrack, A., Gisinger, S., Mixa, T., Reichert, R., Kaifler, N., Knobloch, S., Eckert, R., Wildmann, N., Giez, A., Krasauskas, L., Preusse, P., Geldenhuys, M., Riese, M., Woiwode, W., Friedl-Vallon, F., Sinnhuber, B.-M., La Torre, A. d., Alexander, P., Hormaechea, J. L., Janches, D., Garhammer, M., Chau, J. L., Conte, J. F., Hoor, P., and Engel, A.: SOUTHTRAC-GW: An Airborne Field

500   Campaign to Explore Gravity Wave Dynamics at the World's Strongest Hotspot, Bulletin of the American Meteorological Society, 102, E871–E893, https://doi.org/10.1175/BAMS-D-20-0034.1, 2021.

Riese, M., Ploeger, F., Rap, A., Vogel, B., Konopka, P., Dameris, M., and Forster, P.: Impact of uncertainties in atmospheric mixing on simulated UTLS composition and related radiative effects, Journal of Geophysical Research: Atmospheres, 117, https://doi.org/10.1029/2012JD017751, 2012.

505 Riese, M., Oelhaf, H., Preusse, P., Blank, J., Ern, M., Friedl-Vallon, F., Fischer, H., Guggenmoser, T., Höpfner, M., Hoor, P., Kaufmann, M., Orphal, J., Plöger, F., Spang, R., Suminska-Ebersoldt, O., Ungermann, J., Vogel, B., and Woiwode, W.: Gimballed Limb Observer for Radiance Imaging of the Atmosphere (GLORIA) scientific objectives, Atmospheric Measurement Techniques, 7, 1915–1928, https://doi.org/10.5194/amt-7-1915-2014, 2014.

Rinsland, C. P., Dufour, G., Boone, C. D., Bernath, P. F., and Chiou, L.: Atmospheric Chemistry Experiment (ACE) measurements of elevated

510   Southern Hemisphere upper tropospheric CO, C2H6, HCN, and C2H2 mixing ratios from biomass burning emissions and long-range transport, Geophysical Research Letters, 32, https://doi.org/10.1029/2005GL024214, 2005.

Rolph, G., Stein, A., and Stunder, B.: Real-time Environmental Applications and Display sYstem: READY, Environmental Modelling & Software, 95, 210–228, https://doi.org/10.1016/j.envsoft.2017.06.025, 2017.

Rothman, L. S., Jacquemart, D., Barbe, A., Benner, D. C., Birk, M., Brown, L. R., Carleer, M. R., Chackerian, C., Chance, K., Coudert,

515   L. H., Dana, V., Devi, V. M., Flaud, J. M., Gamache, R. R., Goldman, A., Hartmann, J. M., Jucks, K. W., Maki, A. G., Mandin, J. Y., Massie, S. T., Orphal, J., Perrin, A., Rinsland, C. P., Smith, M. A. H., Tennyson, J., Tolchenov, R. N., Toth, R. A., Auwera, J. V., Varanasi, P., and Wagner, G.: The HITRAN 2004 molecular spectroscopic database, Journal of Quantitative Spectroscopy and Radiative Transfer, 96, 139–204, https://doi.org/10.1016/j.jqsrt.2004.10.008, http://www.sciencedirect.com/science/article/pii/S0022407305001081, 2005.

Rudolph, J.: The tropospheric distribution and budget of ethane, Journal of Geophysical Research: Atmospheres, 100, 11 369–11 381,

520   https://doi.org/10.1029/95JD00693, 1995.

Rémy, S., Veira, A., Paugam, R., Sofiev, M., Kaiser, J. W., Marenco, F., Burton, S. P., Benedetti, A., Engelen, R. J., Ferrare, R., and Hair, J. W.: Two global data sets of daily fire emission injection heights since 2003, Atmospheric Chemistry and Physics, 17, 2921–2942, https://doi.org/10.5194/acp-17-2921-2017, 2017.

Sawada, S. and Totsuka, T.: Natural and anthropogenic sources and fate of atmospheric ethylene, Atmospheric Environment (1967), 20,

525   821–832, https://doi.org/10.1016/0004-6981(86)90266-0, 1986.

Singh, H., Chen, Y., Staudt, A., Jacob, D., Blake, D., Heikes, B., and Snow, J.: Evidence from the Pacific troposphere for large global sources of oxygenated organic compounds, Nature, 410, 1078, https://doi.org/10.1038/35074067, 2001.

Stein, A. F., Draxler, R. R., Rolph, G. D., Stunder, B. J. B., Cohen, M. D., and Ngan, F.: NOAA's HYSPLIT Atmospheric Transport and Dispersion Modeling System, Bulletin of the American Meteorological Society, 96, 2059–2077, https://doi.org/10.1175/BAMS-D-14-

530   00110.1, 2015.

Torres, O., Chen, Z., Jethva, H., Ahn, C., Freitas, S. R., and Bhartia, P. K.: OMI and MODIS observations of the anomalous 2008–2009
Southern Hemisphere biomass burning seasons, Atmospheric Chemistry and Physics, 10, 3505–3513, https://doi.org/10.5194/acp-10-
3505-2010, 2010.

Ungermann, J., Pan, L. L., Kalicinsky, C., Olschewski, F., Knieling, P., Blank, J., Weigel, K., Guggenmoser, T., Stroh, F., Hoffmann, L., and

535   Riese, M.: Filamentary structure in chemical tracer distributions near the subtropical jet following a wave breaking event, Atmospheric
Chemistry and Physics, 13, 10 517–10 534, https://doi.org/10.5194/acp-13-10517-2013, 2013.

Ungermann, J., Kleinert, A., Maucher, G., Bartolomé, I., Friedl-Vallon, F., Johansson, S., Krasauskas, L., and Neubert, T.: Quantification
and mitigation of the airborne limb imaging FTIR GLORIA instrument effects and uncertainties, Atmospheric Measurement Techniques
Discussions, pp. 1–69, https://doi.org/10.5194/amt-2021-293, https://amt.copernicus.org/preprints/amt-2021-293/, 2021.

540   van der Werf, G. R., Randerson, J. T., Giglio, L., van Leeuwen, T. T., Chen, Y., Rogers, B. M., Mu, M., van Marle, M. J. E., Morton, D. C.,
Collatz, G. J., Yokelson, R. J., and Kasibhatla, P. S.: Global fire emissions estimates during 1997–2016: Earth System Science Data, 9(2),
697-720, Earth System Science Data, 9, 697–720, https://doi.org/10.5194/ESSD-9-697-2017, 2017.

Wang, Y., Ma, Y.-F., Eskes, H., Inness, A., Flemming, J., and Brasseur, G. P.: Evaluation of the CAMS global atmospheric
trace gas reanalysis 2003–2016 using aircraft campaign observations, Atmospheric Chemistry and Physics, 20, 4493–4521,

545   https://doi.org/10.5194/acp-20-4493-2020, 2020.

Wetzel, G., Friedl-Vallon, F., Glatthor, N., Grooß, J.-U., Gulde, T., Höpfner, M., Johansson, S., Khosrawi, F., Kirner, O., Kleinert, A.,
Kretschmer, E., Maucher, G., Nordmeyer, H., Oelhaf, H., Orphal, J., Piesch, C., Sinnhuber, B.-M., Ungermann, J., and Vogel, B.: Pollution
trace gases C_2H_6, C_2H_2, HCOOH, and PAN in the North Atlantic UTLS: observations and simulations, Atmospheric Chemistry and
Physics, 21, 8213–8232, https://doi.org/10.5194/acp-21-8213-2021, 2021.

550   Wiegele, A., Glatthor, N., Höpfner, M., Grabowski, U., Kellmann, S., Linden, A., Stiller, G., and von Clarmann, T.: Global distributions of
C_2H_6, C_2H_2, HCN, and PAN retrieved from MIPAS reduced spectral resolution measurements, Atmospheric Measurement Techniques, 5,
723–734, https://doi.org/10.5194/amt-5-723-2012, 2012.

Wohltmann, I., Lehmann, R., Gottwald, G. A., Peters, K., Protat, A., Louf, V., Williams, C., Feng, W., and Rex, M.: A Lagrangian convective
transport scheme including a simulation of the time air parcels spend in updrafts (LaConTra v1.0), Geoscientific Model Development, 12,

555   4387–4407, https://doi.org/10.5194/gmd-12-4387-2019, 2019.

Xia, Y., Huang, Y., and Hu, Y.: On the Climate Impacts of Upper Tropospheric and Lower Stratospheric Ozone, Journal of Geophysical
Research: Atmospheres, https://doi.org/10.1002/2017JD027398, 2017.

Xiao, Y., Logan, J. A., Jacob, D. J., Hudman, R. C., Yantosca, R., and Blake, D. R.: Global budget of ethane and regional constraints on U.S.
sources, Journal of Geophysical Research: Atmospheres, 113, https://doi.org/10.1029/2007JD009415, 2008.